Electronic Supplementary Information

Binding $MoSe_2$ with Dual Protection Carbon for High-Performance Sodium Storage

Qiong Su, Xinxin Cao,* Ting Yu, Xiangzhong Kong, Yaping Wang, Jing Chen, Jiande Lin, Xuefang Xie, Shuquan Liang and Anqiang Pan*

School of Materials Science and Engineering, Central South University, Changsha 410083, Hunan, China

* Corresponding authors: caoxinxin@csu.edu.cn (X. Cao), pananqiang@csu.edu.cn (A. Pan)

Experimental

Materials synthesis

1. Synthesis of organic-inorganic hybrid material of MoO_x-EDA nanorods

All chemicals and reagents were used directly without any treatment. The organic-inorganic hybrid material MoO_x-EDA nanorods were similarly prepared referring to previous reports[1-5]. Typically, ethylenediamine (EDA) (0.93 mL, 14 mmol) was added to a solution of ammonium heptamolybdate ($(NH_4)_6Mo_7O_{24}\cdot 4H_2O$) (1.24 g, 1 mmol) in deionized water (20 mL) at room temperature. After that, 1 M HCl aqueous solution was dripped into the system slowly with magnetic stirring until a white precipitate appeared (PH 4~5). Then, the reaction was transferred to an oil bath and heat to 50 °C for 4 h. The obtained product was filtered and washed three times with deionized water and then dried at 50 °C for 24 h.

2. Synthesis of MoO_x-EDA@PDDA@GO composite

GO was obtained from commercial purchase. Poly dimethyl diallyl ammonium chloride (PDDA) in deionized water solution (4 mL, 1 wt. %) was added into GO suspension (10 mL, ~ 5.0 mg mL^{-1}), which was processed ultrasound for 6 h, and then stirred for 1 h.

MoO_x-EDA@PDDA@GO-200: The as-prepared organic-inorganic hybrid material of MoO_x-EDA nanorods (200 mg) were dispersed in the above GO with PDDA by stirring for 40 min and then sonicated for 15 min. The obtained mixture was frozen and dried in a freezer dryer for 24 h.

MoO_x-EDA@PDDA@GO-25, MoO_x-EDA@PDDA@GO-50 and MoO_x-EDA@PDDA@GO-400 were prepared similarly as MoO_x-EDA@PDDA@GO-200,

excepting that the mass of MoO_x-EDA is 25, 50, 400 mg, respectively.

3. Synthesis of $MoSe_2$@NC@rGO

$MoSe_2$@NC@rGO-200: The as-obtained fluffy earthy yellow organic-inorganic hybrid of MoO_x-EDA@PDDA@GO-200 (134 mg) and Se powder (150 mg) were mixed in a quartz boat in a tube furnace. Afterwards, the temperature was raised to 600 °C and kept it for 2 h to complete the reaction under H_2/Ar flow (5%/95%). The heating ramping rate was 3 °C min^{-1}. Then, the target product, $MoSe_2$@NC@rGO-200 composite was obtained.

$MoSe_2$@NC@rGO-25, $MoSe_2$@NC@rGO-50 and $MoSe_2$@NC@rGO-400 were prepared at the same condition as $MoSe_2$@NC@rGO-200, excepting that the starting materials are MoO_x-EDA@PDDA@GO-25, MoO_x-EDA@PDDA@GO-50 and MoO_x-EDA@PDDA@GO-400, respectively.

4. Synthesis of $MoSe_2$ nanorods

The as-obtained organic-inorganic hybrid of MoO_x-EDA (200 mg, 0.39 mmol) and Se powder (280 mg, 3.55 mmol) were placed in a quartz boat in a tube furnace. Then, the temperature was raised to 600 °C and kept it for 2 h to complete the reaction under H_2/Ar flow (5%/95%). The heating rate was set of 3 °C min^{-1}.

5. Synthesis of rGO

GO solution from commercial purchase was first frozen and dried in a freezer dryer for 24 h. Afterwards, the fluffy brown freeze-dried GO (150 mg) was placed in a quartz boat in a tube furnace. Then, the temperature was raised to 600 °C and kept at this temperature for 2 h to finish the reaction under H_2/Ar flow (5%/95%). The heating rate was 3 °C min^{-1}.

Characterization

The crystallographic phases of the samples were measured by X-ray diffraction (XRD, Rigaku D/max 2500, Cu-Kα, λ = 1.54178 Å). Fourier transform infrared (FT-IR) spectra were obtained using an FT-IR spectrometer (Nicolet 6700). The characteristic bands of $MoSe_2$, GO and rGO and graphitization degree of samples were analyzed by Raman spectrometer (LabRAM HR800). The weight percentages of $MoSe_2$ in the composite were analyzed by thermogravimetric (TG, Netzsch, STA 449C), which were conducted in air from 25 to 700 °C with a heating ramp rate of 10 °C min^{-1}. The existence and valence of the element in the composite were identified by X-ray photoelectron spectroscopy spectrum (XPS, ESCALAB 250Xi). The morphologies and microstructures of samples were characterized by a field-emission scanning electron microscope (FESEM, FEI Nova NanoSEM 230), a high-resolution transmission electron microscope (HRTEM, Titan G2 60-300), the selected area electron diffraction (SAED) pattern and high angle annular dark field scanning transmission electron microscopy (HAADF-STEM).

Electrode fabrication and electrochemical measurements

The anode was prepared by grinding the active materials (70 wt. %), super P (20 wt. %) and Carboxy Methyl Cellulose (CMC, 10 wt. %) binder, adding deionized water to get a viscous slurry, and then coating the slurry on Cu foil and dried in vacuum at 80 °C for 12 h. The diameter of each electrode is 12 mm and the active material loading of each plate is about 0.7-1.0 mg. The electrochemical performances of $MoSe_2$@NC@rGO, $MoSe_2$ and rGO were evaluated via CR2016 coin cells. All batteries were assembled in a glove box (Shanghai MIKROUNA) filled with ultra-high pure argon. The glass microfiber filters (Whatman GF/D) were employed as separator and 1 M $NaClO_4$ in propylene carbonate (PC) and fluoroethylene

carbonate (FEC) mixture solution (95: 5 in volume) were used as electrolyte. For half cells, Na plate was served as countered electrode. The voltage during the discharge/charge process was set at the range of 0.01 and 3.0 V. For Na-ion full cells, the cathode is made of $(Na_3V_2(PO_4)_3/C$ (75 wt. %), super P (15 wt. %) and polyvinylidene (PVDF, 10 wt. %) binder on an Al foil. Prior to full cells fabrication, one cycle activation of $MoSe_2$@NC@rGO anode was performed. The capacity ratio for cathode and anode was controlled around 1.1:1. The voltage during the discharge and charge process was set between 1.0 and 3.5 V for the full-cell. All the electrochemical measurements of the as-assembled batteries were tested on a Land Battery Tester (Land CT2001A). Cyclic voltammetry (CV) was conducted on an electrochemical workstation (CHI660E, Shanghai Chenhua Instrument Co., China) between 0.01 to 3.0 V. The electrochemical impedance spectroscopy (EIS) were recorded on an electrochemical workstation (ZAHNER-IM6ex, ZAHNER Co., Germany) in the frequency range of 10^5 Hz to 0.01 Hz.

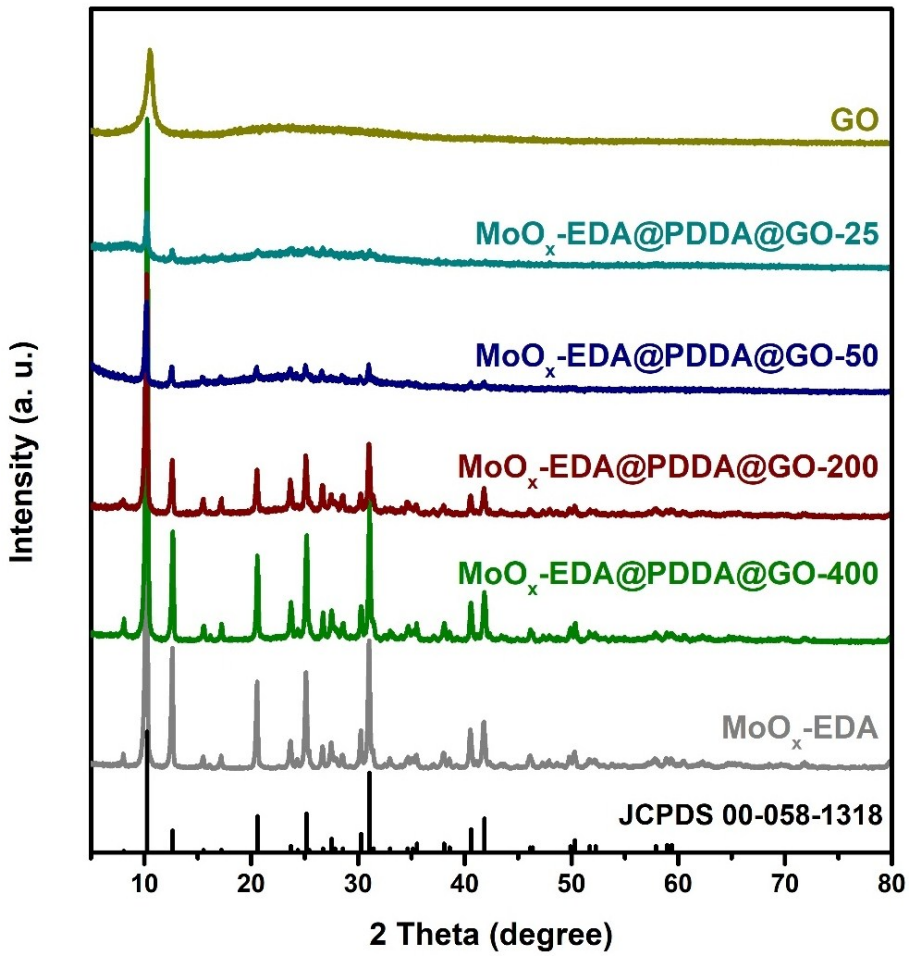

Fig. S1. XRD patterns of MoO_x-EDA@PDDA@GO composites, MoO_x-EDA and GO.

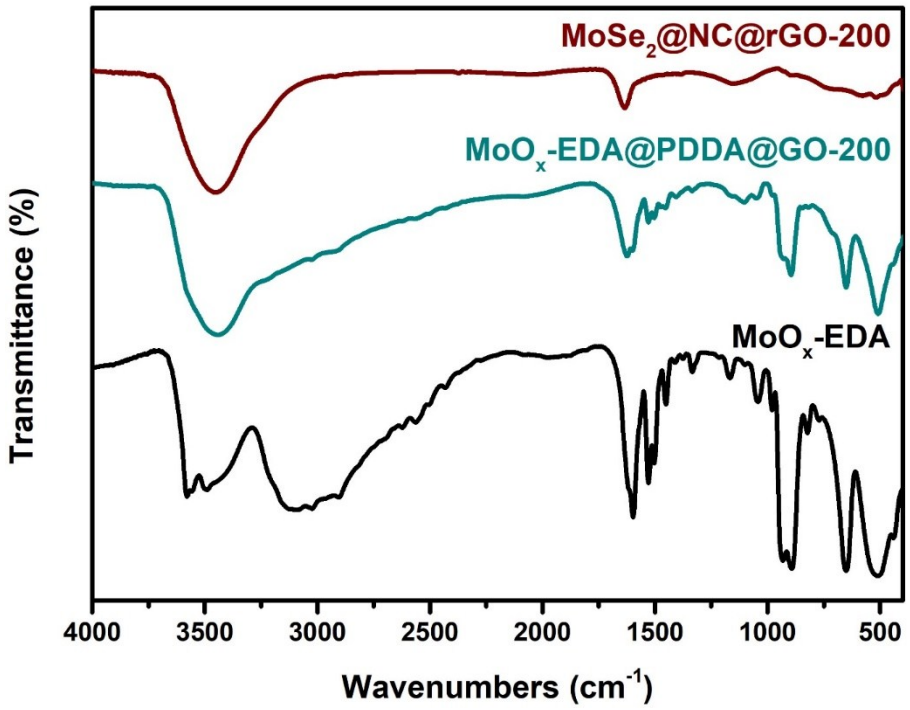

Fig. S2. FT-IR spectra of MoO_x-EDA, MoO_x-EDA@PDDA@GO-200 and $MoSe_2$@NC@rGO-200.

For MoO_x-EDA, the absorption peak in IR around 1597, 1529 and 1503 cm^{-1} are assigned to ν_{NH3+}, and the peak around 1167 cm^{-1} is due to ν_{C-N}[3]. Besides, ν_{Mo-O} and $\nu_{Mo=O}$ are also detected around 509, 893 and 931 cm^{-1}[6]. With the addition of GO and PDDA, the spectrum of MoO_x-EDA@PDDA@GO-200 has changed slightly. After selenization, the above peaks are disappeared in $MoSe_2$@NC@rGO-200 IR spectra, suggesting that the MoO_x-EDA@PDDA@GO-200 precursor has been successfully transformed into $MoSe_2$@NC@rGO-200[7-9].

Note S1.

According to Mo element conservation, the following equation (Eq. S1) is obtained, in which $\bar{M}_{MoSe_2}$ and $\bar{M}_{MoO_3}$ stand for the average molecular weight of $MoSe_2$ and MoO_3 respectively, and $M_{MoO_3}\%$ represents the percentage containing of MoO_3 in the system.

$$M_{MoSe_2}\% = \frac{\bar{M}_{MoSe_2}}{\bar{M}_{MoO_3}} \times M_{MoO_3}\% \quad \text{(Eq. S1)}$$

$\bar{M}_{MoSe_2}$ = 253.86, $\bar{M}_{MoO_3}$ = 143.94, $M_{MoO_3}\%$ equals 56%, 49%, 46% and 31% for $MoSe_2$@NC@rGO-400, $MoSe_2$@NC@rGO-200, $MoSe_2$@NC@rGO-50 and $MoSe_2$@NC@rGO-25, respectively, from TG curves in Fig. 2c. Therefore, the corresponding mass loadings of $MoSe_2$ are estimated to be 98.8%, 86.4%, 81.1%, 54.7%.

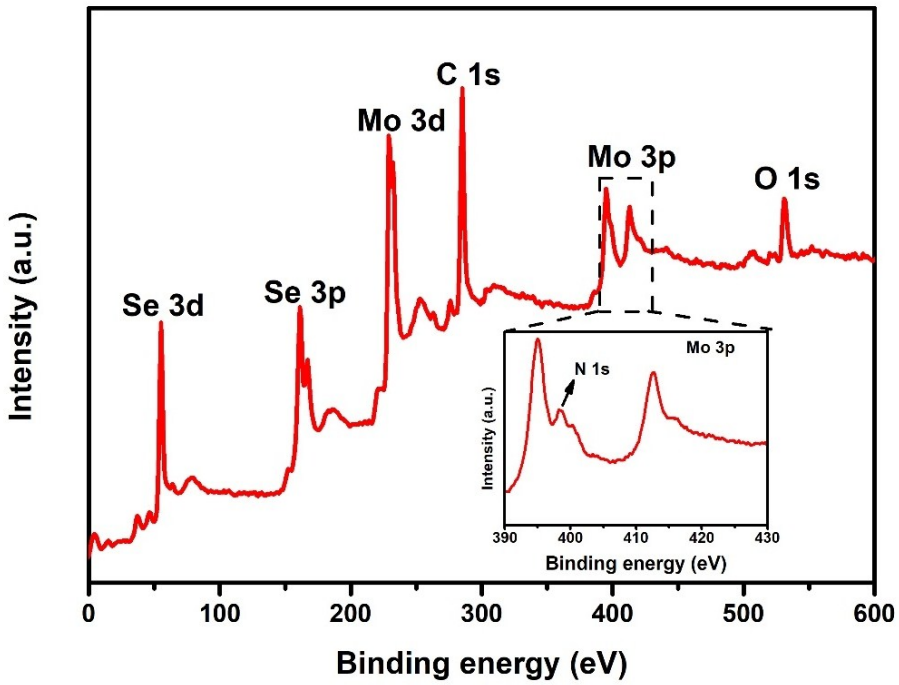

Fig. S3. Survey spectrum of $MoSe_2$@NC@rGO-200.

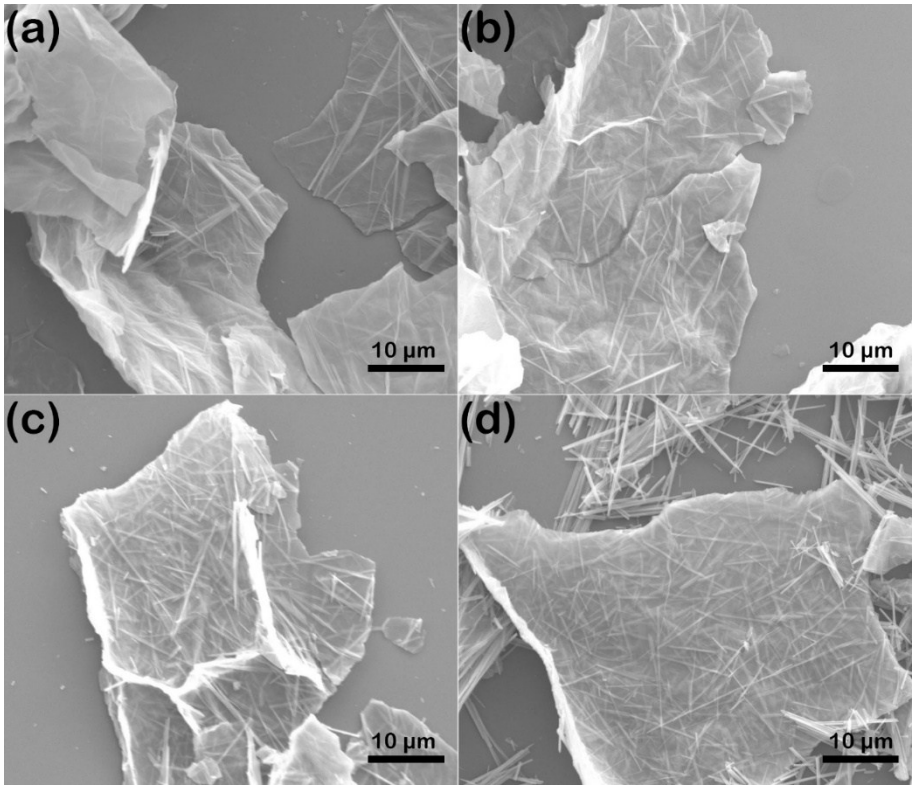

Fig. S4. SEM images of (a) MoO_x-EDA@PDDA@GO-25, (b) MoO_x-EDA@PDDA@GO-50, (c) MoO_x-EDA@PDDA@GO-200, (d) MoO_x-EDA@PDDA@GO-400.

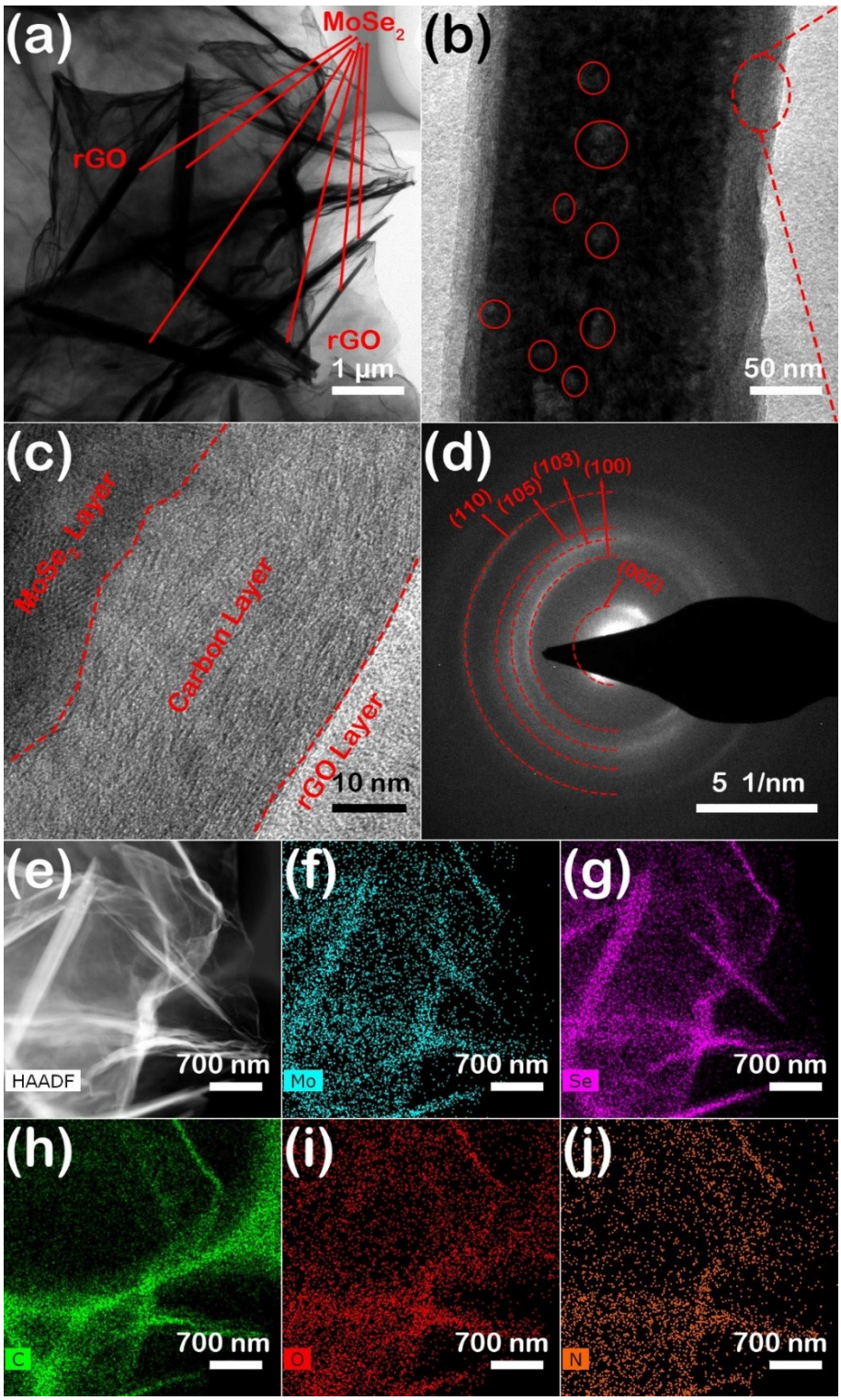

Fig. S5. (a, b) TEM images; (c) HRTEM images; (d) SAED pattern; (e-j) HAADF-STEM images (Mo, Se, C, O, N) of $MoSe_2$@NC@rGO-50.

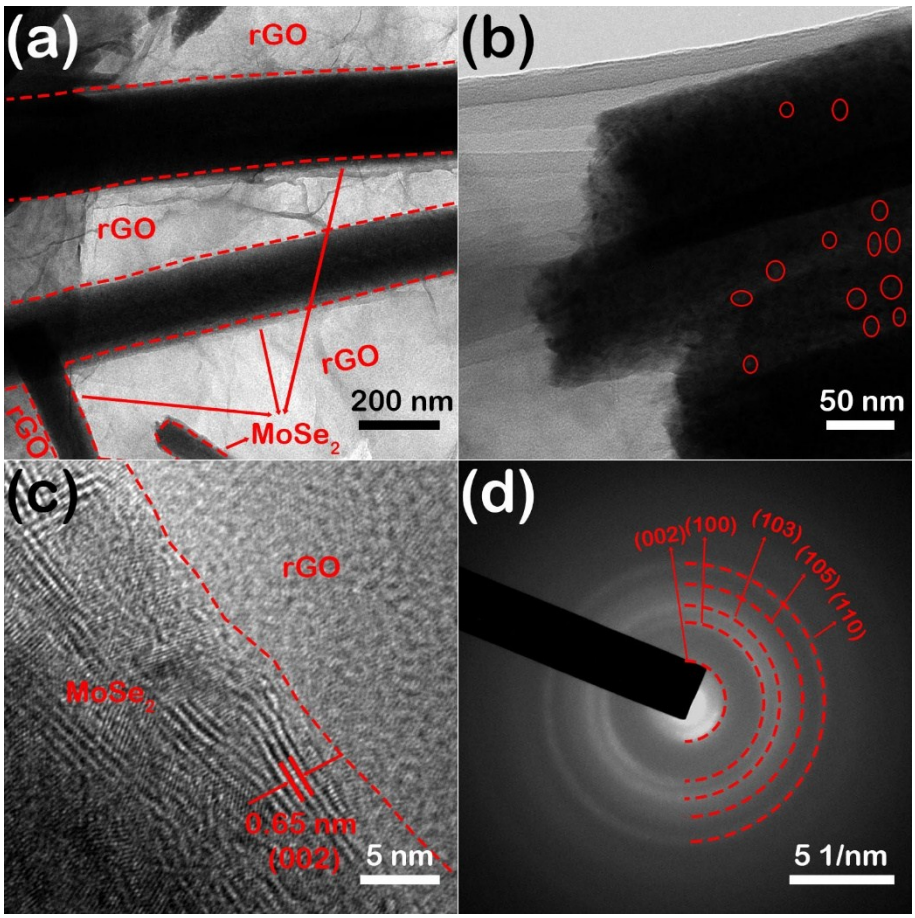

Fig. S6. (a, b) TEM images; (c) HRTEM images; (d) SAED pattern of $MoSe_2$@NC@rGO-400.

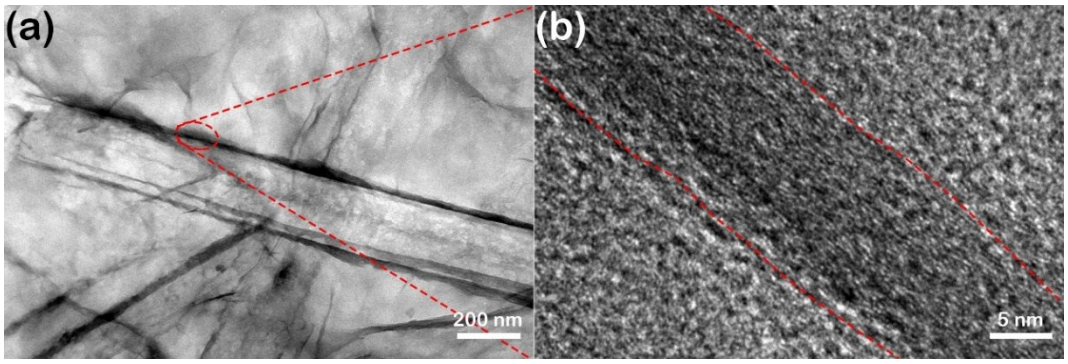

Fig. S7. (a) TEM images; (b) HRTEM images of $MoSe_2$@NC@rGO-200 treated with the mixture of HCl (37%) and HNO_3 (68%) (3:1 in volume).

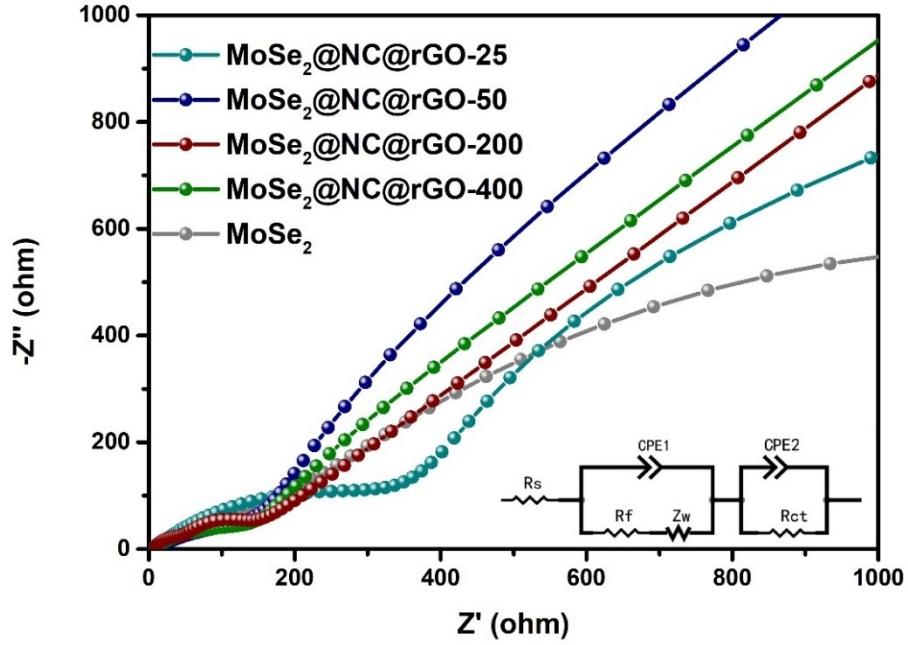

Fig. S8. Nyquist plots of $MoSe_2$@NC@rGO composites and $MoSe_2$ at 100 mA g^{-1} after 5 cycles. The bottom inset is the corresponding equivalent circuit model.

The equivalent circuit model is composed of R_s (electrolyte resistance), R_f (the SEI layer resistance), CPE1 (the constant phase element), Z_w (the Warburg impedance), R_{ct} (the charge transfer resistance) and CPE2 (double layer capacitor)[10-13].

Table S1 The primary impedance fitting parameters of $MoSe_2$@NC@rGO composites and $MoSe_2$ after 5 cycles

Sample	R_f	R_{ct}
$MoSe_2$@NC@rGO-25	972.7	415.5
$MoSe_2$@NC@rGO-50	354	222.9
$MoSe_2$@NC@rGO-200	43.74	63.5
$MoSe_2$@NC@rGO-400	158.6	196.6
$MoSe_2$	1975	169.1

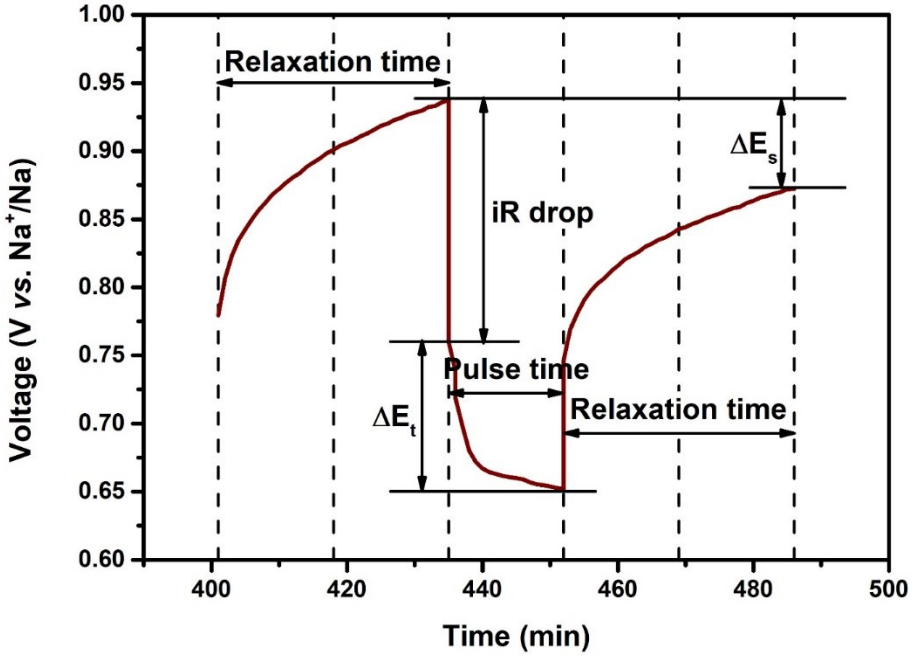

Fig. S9. E vs. t curves of $MoSe_2$@NC@rGO-200 composite electrode for a single GITT during discharge process.

Note S2.

The Na^+ diffusion coefficient (D) was tested by galvanostatic intermittent titration technique (GITT) and calculated based on Eq. S2 as follows:

$$D = \frac{4L^2}{\pi\tau}\left(\frac{\Delta E_s}{\Delta E_t}\right)^2 \qquad \text{(Eq. S2)}$$

Where t represents the duration of the current pulse (s). τ represents the relaxation time (s), and ΔE_s represents the steady-state voltage change (V) by the current pulse. ΔE_t represents the voltage change (V) during the constant current pulse after eliminating the iR drop. L represents Na^+ diffusion length (cm), it equals to the thickness of electrode[14, 15].

During GITT process, $MoSe_2$@NC@rGO-200 anode was charged/discharged utilizing a current pulse of 100 mA g^{-1} for 1020 s (pulse time), and then rested for 2040 s (relaxation

time). This is repeated until the cut-off potential is reached. In the GITT curve, the fast voltage variation (iR drop) is indexed to the charge transfer and ohm resistance, and the slow variation should be ascribed to the ion diffusion.

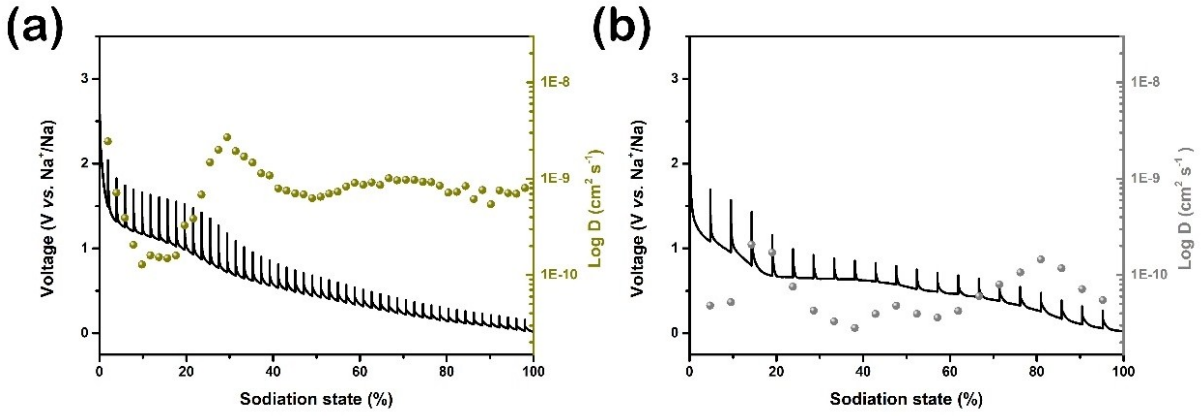

Fig. S10. GITT curves and the corresponding Na^+ diffusion coefficient at different sodiation state of (a) rGO and (b) $MoSe_2$ electrodes.

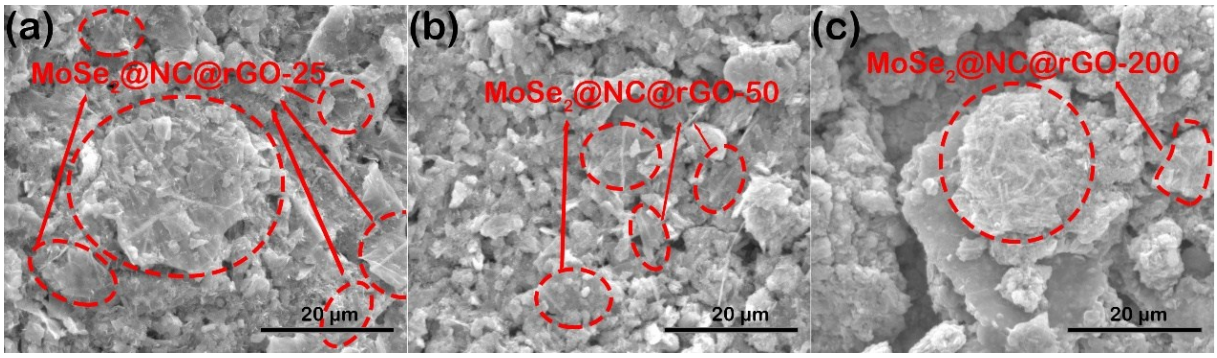

Fig. S11. SEM images after 200 cycles at 1000 mA g^{-1} for (a) $MoSe_2$@NC@rGO-25; (b) $MoSe_2$@NC@rGO-50; (c) $MoSe_2$@NC@rGO-200.

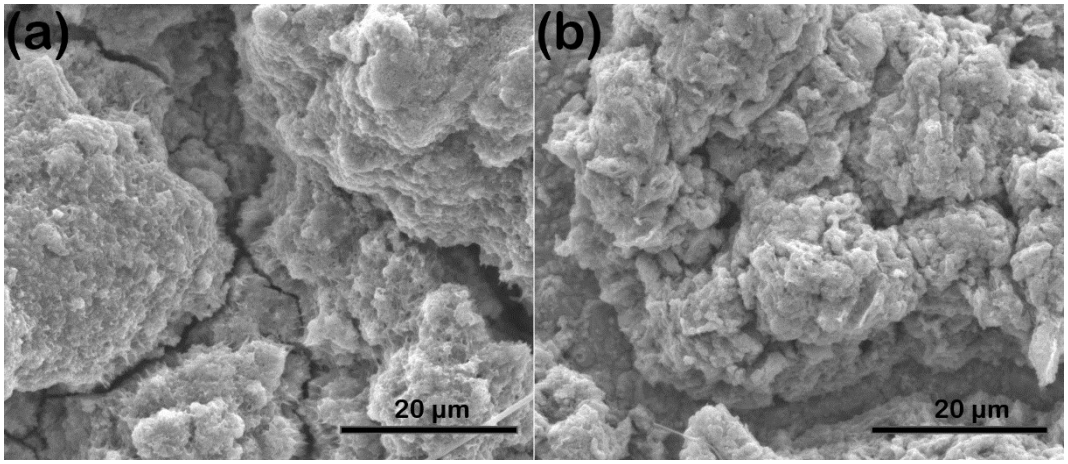

Fig. S12. SEM images after 200 cycles at 1000 mA g^{-1} for (a) $MoSe_2$@NC@rGO-400; (b) $MoSe_2$.

Table S2 A comparison of electrochemical performances of some previous reports about $MoSe_2$-base anode materials with our results for SIBs in half-cell and full-cell

Anode Materials	Cycling properties			Rate properties		full cell (mA h g^{-1}) (Cycle number, Current density)	Year/Ref.
	Capacity (mA h g^{-1})	Cycle number	Current density (mA g^{-1})	Capacity (mA h g^{-1})	Current density (mA g^{-1})		
$MoSe_2$@NC@rGO	438	100	100	312	2000	300 (100 mA g^{-1})	This work
	360	200	1000	281	5000	208 (100, 1000 mA g^{-1})	
$MoSe_2$@$CoSe_2$/N-C composite	485	100	100	393	2000	345 (100 mA g^{-1})	2018[6]
	347	300	2000			197 (100, 2000 mA g^{-1})	
$MoSe_2$/C composite	404	100	200	192	5000	—	2018[1]
$MoSe_2$@N-C nanospheres	552	120	100	530	1000	—	2018[10]
				238	8000		
$MoSe_2$/HPCFs	347	100	100	243	2000	—	2018[16]
$MoSe_2$-N,P-doped rGO composites	337	100	100	223	1000	—	2018[17]
$MoSe_2$-rGO-CNT	393	200	1000	314	2000	—	2017[18]
				275	5000		
$MoSe_2$/N,P-rGO	378	1000	500	351	1000	276 (200, 500 mA g^{-1})	2017[19]
				310	5000		
Flower-like $MoSe_2$/C composite	360	350	500	301	2000	—	2017[20]
				266	4000		
$MoSe_2$@C@GR	367	200	200	320	2000	—	2017[21]
$MoSe_2$/N-C nanosphere	334	500	500	248	2000		2017[22]
				180	5000		
$MoSe_2$@C	445	100	1000	367	5000	421 (100, 200 mA g^{-1})	2016[8]
VG/$MoSe_2$/N-C sandwiched arrays	534	400	200	300	2000	—	2016[23]
coaxial-cable	423	100	500	359	2000	—	2016[24]
$MoSe_2$/C composites	395	100	1000				
$MoSe_2$ nanosphere	345	200	42.2 (0.1 C)	212	4223	—	2016[25]
C-$MoSe_2$/rGO composite	445	350	200	284	2000	—	2016[26]
				228	4000		
F-$MoSe_2$/CNT composite balls	296	250	1000	280	3000	—	2016[27]
				255	5000		
$MoSe_2$/CF	387	100	200	240	2000	—	2016[28]

				162	5000		
$MoSe_2$/rGO composite	430	200	500	380	1000	—	2015[9]
$MoSe_2$ nanoplates	369	50	42.2 (0.1 C)	250	4223 (10 C)	—	2015[12]
$MoSe_2$@MWCNT	459	90	200	385	2000	—	2015[29]
$MoSe_2$@PHCS	580	100	200	400	1500	—	2015[30]
$MoSe_2$ yolk-shell microspheres	433	50	200	345	1500	—	2014[31]

References

1. Q. Su, X. Cao, X. Kong, Y. Wang, C. Peng, J. Chen, B. Yin, J. Shi, S. Liang and A. Pan, *Electrochimi. Acta*, 2018, **292**, 339-346.
2. Q. Gao, S. Wang, H. Fang, J. Weng, Y. Zhang, J. Mao and Y. Tang, *J. Mater. Chem.*, 2012, **22**, 4709.
3. S. Zhuo, Y. Xu, W. Zhao, J. Zhang and B. Zhang, *Angew. Chem. Int. Ed. Engl.*, 2013, **52**, 8602-8606.
4. K. Zhu, X. Wang, J. Liu, S. Lo, H. Wang, L. Yang, S. Liu and T. Xie, *ACS Sustain. Chem. Eng.*, 2017, **5**, 8025-8034.
5. Z. Che, Y. Li, K. Chen and M. Wei, *J. Power Sources*, 2016, **331**, 50-57.
6. J. Chen, A. Pan, Y. Wang, X. Cao, W. Zhang, X. Kong, Q. Su, J. Lin, G. Cao and S. Liang, *Energy Storage Mater.*, 2018, DOI: 10.1016/j.ensm.2018.10.019.
7. C. Dai, Z. Zhou, C. Tian, Y. Li, C. Yang, X. Gao and X. Tian, *J. Phys. Chem. C*, 2017, **121**, 1974-1981.
8. Y. Tang, Z. Zhao, Y. Wang, Y. Dong, Y. Liu, X. Wang and J. Qiu, *ACS Appl. Mater. Inter.*, 2016, **8**, 32324-32332.
9. Z. Zhang, Y. Fu, X. Yang, Y. Qu and Z. Zhang, *ChemNanoMat*, 2015, **1**, 409-414.
10. P. Ge, H. Hou, C. Banks, C. Foster, S. Li, Y. Zhang, J. He, C. Zhang and X. Ji, *Energy Storage Mater.*, 2018, **12**, 310-323.
11. Y. Liu, M. Zhu and D. Chen, *J. Mater. Chem. A*, 2015, **3**, 11857-11862.
12. H. Wang, X. Lan, D. Jiang, Y. Zhang, H. Zhong, Z. Zhang and Y. Jiang, *J. Power Sources*, 2015, **283**, 187-194.

13. Y. Wang, G. Xing, Z. Han, Y. Shi, J. Wong, Z. Huang, K. Ostrikov and H. Yang, *Nanoscale*, 2014, **6**, 8884-8890.
14. G. Fang, Z. Wu, J. Zhou, C. Zhu, X. Cao, T. Lin, Y. Chen, C. Wang, A. Pan and S. Liang, *Adv. Energy Mater.*, 2018, **8**, 1703155.
15. Y. Wang, Y. Zhang, J. shi, X. Kong, X. Cao, S. Liang, G. Cao and A. Pan, *Energy Storage Mater.*, 2019, **18**, 366-374.
16. M. Zhu, Z. Luo, A. Pan, H. Yang, T. Zhu, S. Liang and G. Cao, *Chem. Eng. J.*, 2018, **334**, 2190-2200.
17. A. Roy, A. Ghosh, A. Kumar and S. Mitra, *Inorg. Chem. Front.*, 2018, **5**, 2189-2197.
18. G. Park, J. Kim, S. Park and Y. Kang, *ACS Appl. Mater. Inter.*, 2017, **9**, 10673-10683.
19. F. Niu, J. Yang, N. Wang, D. Zhang, W. Fan, J. Yang and Y. Qian, *Adv. Funct. Mater.*, 2017, **27**, 1700522.
20. J. Li, H. Hu, F. Qin, P. Zhang, L. Zou, H. Wang, K. Zhang and Y. Lai, *Chem. Eur. J.*, 2017, **23**, 14004-14010.
21. C. Cui, G. Zhou, W. Wei, L. Chen, C. Li and J. Yue, *J. Alloy Compd*., 2017, **727**, 1280-1287.
22. G. Jia, H. Wang, D. Chao, H. He, N. H. Tiep, Y. Zhang, Z. Zhang and H. J. Fan, *Nanotechnology*, 2017, **28**, 42LT01.
23. D. Xie, X. Xia, Y. Zhong, Y. Wang, D. Wang, X. Wang and J. Tu, *Adv. Energy Mater.*, 2016, **7**, 1601804.
24. X. Yang, Z. Zhang and X. Shi, *J. Alloy Compd*., 2016, **686**, 413-420.
25. H. Wang, L. Wang, X. Wang, J. Quan, L. Mi, L. Yuan, G. Li, B. Zhang, H. Zhong and Y. Jiang, *J. Electrochem. Soc.*, 2016, **163**, A1627-A1632.
26. D. Xie, W. J. Tang, Y. D. Wang, X. H. Xia, Y. Zhong, D. Zhou, D. H. Wang, X. L. Wang and J. P. Tu, *Nano Res.*, 2016, **9**, 1618-1629.
27. S. Choi and Y. Kang, *Nanoscale*, 2016, **8**, 4209-4216.
28. Y. Zhang, Z. Liu, H. Zhao and Y. Du, *RSC Adv.*, 2016, **6**, 1440-1444.
29. Z. Zhang, X. Yang, Y. Fu and K. Du, *J. Power Sources*, 2015, **296**, 2-9.
30. X. Yang, Z. Zhang, Y. Fu and Q. Li, *Nanoscale*, 2015, **7**, 10198-10203.
31. Y. Ko, S. Choi, S. Park and Y. Kang, *Nanoscale*, 2014, **6**, 10511-10515.